

First combined search for neutrino point-sources in the Southern Hemisphere with the ANTARES and IceCube neutrino telescopes

ANTARES Collaboration: S. Adrián-Martínez¹, A. Albert², M. André³, G. Anton⁴, M. Ardid¹, J.-J. Aubert⁵, B. Baret⁶, J. Barrios-Martí⁷, S. Basa⁸, V. Bertin⁵, S. Biagi⁹, R. Bormuth^{10,11}, M.C. Bouwhuis¹⁰, R. Bruijn^{10,12}, J. Brunner⁵, J. Busto⁵, A. Capone^{13,14}, L. Caramete¹⁵, J. Carr⁵, T. Chiarusi¹⁶, M. Circella¹⁷, R. Coniglione⁹, H. Costantini⁵, P. Coyle⁵, A. Creusot⁶, I. Dekeyser¹⁸, A. Deschamps¹⁹, G. De Bonis^{13,14}, C. Distefano⁹, C. Donzaud^{6,20}, D. Dornic⁵, D. Drouhin², A. Dumas²¹, T. Eberl⁴, D. Elsässer²², A. Enzenhöfer⁴, K. Fehn⁴, I. Felis¹, P. Fermani^{13,14}, F. Folger⁴, L.A. Fusco^{16,23}, S. Galatà⁶, P. Gay²¹, S. Geißelsöder⁴, K. Geyer⁴, V. Giordano²⁴, A. Gleixner⁴, R. Gracia-Ruiz⁶, K. Graf⁴, S. Hallmann⁴, H. van Haren²⁵, A.J. Heijboer¹⁰, Y. Hello¹⁹, J.J. Hernández-Rey⁷, J. Höfl⁴, J. Hofestädt⁴, C. Hugon^{26,27}, C.W James⁴, M. de Jong^{10,11}, M. Kadler²², O. Kalekin⁴, U. Katz⁴, D. Kießling⁴, P. Kooijman^{10,28,12}, A. Kouchner⁶, M. Kreter²², I. Kreykenbohm²⁹, V. Kulikovskiy^{9,30}, R. Lahmann⁴, D. Lefèvre¹⁸, E. Leonora^{24,31}, S. Loucatos³², M. Marcellin⁸, A. Margiotta^{16,23}, A. Marinelli^{33,34}, J.A. Martínez-Mora¹, A. Mathieu⁵, T. Michael¹⁰, P. Migliozzi³⁵, A. Moussa³⁶, C. Mueller²², E. Nezri⁸, G.E. Pávālas¹⁵, C. Pellegrino^{16,23}, C. Perrina^{13,14}, P. Piattelli⁹, V. Popa¹⁵, T. Pradier³⁷, C. Racca², G. Riccobene⁹, R. Richter⁴, K. Roensch⁴, M. Saldaña¹, D. F. E. Samtleben^{10,11}, A. Sánchez-Losa⁷, M. Sanguineti^{26,27}, P. Sapienza⁹, J. Schmid⁴, J. Schnabel⁴, F. Schüssler³², T. Seitz⁴, C. Sieger⁴, M. Spurio^{16,23}, J.J.M. Steijger¹⁰, Th. Stolarczyk³², M. Taiuti^{26,27}, C. Tamburini¹⁸, A. Trovato⁹, M. Tselengidou⁴, C. Tönnis⁷, B. Vallage³², C. Vallée⁵, V. Van Elewyck⁶, E. Visser¹⁰, D. Vivolo^{35,38}, S. Wagner⁴, J. Wilms²⁹, J.D. Zornoza⁷, J. Zúñiga⁷

IceCube Collaboration: M. G. Aartsen³⁹, K. Abraham⁴⁰, M. Ackermann⁴¹, J. Adams⁴², J. A. Aguilar⁴³, M. Ahlers⁴⁴, M. Ahrens⁴⁵, D. Altmann⁴⁶, T. Anderson⁴⁷, I. Anseau⁴³, M. Archinger⁴⁸, C. Argüelles⁴⁴, T. C. Arlen⁴⁷, J. Auffenberg⁴⁹, X. Bai⁵⁰, S. W. Barwick⁵¹, V. Baum⁴⁸, R. Bay⁵², J. J. Beatty^{53,54}, J. Becker Tjus⁵⁵, K.-H. Becker⁵⁶, E. Beiser⁴⁴, P. Berghaus⁴¹, D. Berley⁵⁷, E. Bernardini⁴¹, A. Bernhard⁴⁰, D. Z. Besson⁵⁸, G. Binder^{59,52}, D. Bindig⁵⁶, M. Bissok⁴⁹, E. Blaufuss⁵⁷, J. Blumenthal⁴⁹, D. J. Boersma⁶⁰, C. Boehm⁴⁵, M. Börner⁶¹, F. Bos⁵⁵, D. Bose⁶², S. Böser⁴⁸, O. Botner⁶⁰, J. Braun⁴⁴, L. Brayeur⁶³, H.-P. Bretz⁴¹, N. Buzinsky⁶⁴, J. Casey⁶⁵, M. Casier⁶³, E. Cheung⁵⁷, D. Chirkin⁴⁴, A. Christov⁶⁶, K. Clark⁶⁷, L. Classen⁴⁶, S. Coenders⁴⁰, D. F. Cowen^{47,68}, A. H. Cruz Silva⁴¹, J. Daughhetee⁶⁵, J. C. Davis⁵³, M. Day⁴⁴, J. P. A. M. de André⁶⁹, C. De Clercq⁶³, E. del Pino Rosendo⁴⁸, H. Dembinski⁷⁰, S. De Ridder⁷¹, P. Desiati⁴⁴, K. D. de Vries⁶³, G. de Wasseige⁶³, M. de With⁷², T. DeYoung⁶⁹, J. C. Díaz-Vélez⁴⁴, V. di Lorenzo⁴⁸, J. P. Dumm⁴⁵, M. Dunkman⁴⁷, B. Eberhardt⁴⁸, T. Ehrhardt⁴⁸, B. Eichmann⁵⁵, S. Euler⁶⁰, P. A. Evenson⁷⁰, S. Fahey⁴⁴, A. R. Fazely⁷³, J. Feintzeig⁴⁴, J. Felde⁵⁷, K. Filimonov⁵², C. Finley⁴⁵, T. Fischer-Wasels⁵⁶, S. Flis⁴⁵, C.-C. Fösig⁴⁸, T. Fuchs⁶¹, T. K. Gaisser⁷⁰, R. Gaior⁷⁴, J. Gallagher⁷⁵, L. Gerhardt^{59,52}, K. Ghorbani⁴⁴, D. Gier⁴⁹, L. Gladstone⁴⁴, M. Glagla⁴⁹, T. Glüsenskamp⁴¹, A. Goldschmidt⁵⁹, G. Golup⁶³, J. G. Gonzalez⁷⁰, D. Góra⁴¹, D. Grant⁶⁴, Z. Griffith⁴⁴, A. Groß⁴⁰, C. Ha^{59,52}, C. Haack⁴⁹, A. Haj Ismail⁷¹, A. Hallgren⁶⁰, F. Halzen⁴⁴, E. Hansen⁷⁶, B. Hansmann⁴⁹,

K. Hanson⁴⁴, D. Hebecker⁷², D. Heereman⁴³, K. Helbing⁵⁶, R. Hellauer⁵⁷, S. Hickford⁵⁶,
J. Hignight⁶⁹, G. C. Hill³⁹, K. D. Hoffman⁵⁷, R. Hoffmann⁵⁶, K. Holzapfel⁴⁰, A. Homeier⁷⁷,
K. Hoshina^{44,87}, F. Huang⁴⁷, M. Huber⁴⁰, W. Huelsnitz⁵⁷, P. O. Hulth⁴⁵, K. Hultqvist⁴⁵, S. In⁶²,
A. Ishihara⁷⁴, E. Jacobi⁴¹, G. S. Japaridze⁷⁸, M. Jeong⁶², K. Jero⁴⁴, M. Jurkovic⁴⁰, A. Kappes⁴⁶,
T. Karg⁴¹, A. Karle⁴⁴, M. Kauer^{44,79}, A. Keivani⁴⁷, J. L. Kelley⁴⁴, J. Kemp⁴⁹, A. Kheirandish⁴⁴,
J. Kiryluk⁸⁰, J. Kläs⁵⁶, S. R. Klein^{59,52}, G. Kohnen⁸¹, R. Koirala⁷⁰, H. Kolanoski⁷², R. Konietz⁴⁹,
L. Köpke⁴⁸, C. Kopper⁶⁴, S. Kopper⁵⁶, D. J. Koskinen⁷⁶, M. Kowalski^{72,41}, K. Krings⁴⁰,
G. Kroll⁴⁸, M. Kroll⁵⁵, G. Krücl⁴⁸, J. Kunnen⁶³, N. Kurahashi⁸², T. Kuwabara⁷⁴, M. Labare⁷¹,
J. L. Lanfranchi⁴⁷, M. J. Larson⁷⁶, M. Lesiak-Bzdak⁸⁰, M. Leuermann⁴⁹, J. Leuner⁴⁹, L. Lu⁷⁴,
J. Lünemann⁶³, J. Madsen⁸³, G. Maggi⁶³, K. B. M. Mahn⁶⁹, M. Mandelartz⁵⁵, R. Maruyama⁷⁹,
K. Mase⁷⁴, H. S. Matis⁵⁹, R. Maunu⁵⁷, F. McNally⁴⁴, K. Meagher⁴³, M. Medici⁷⁶, A. Meli⁷¹,
T. Menne⁶¹, G. Merino⁴⁴, T. Meures⁴³, S. Miarecki^{59,52}, E. Middell⁴¹, L. Mohrmann⁴¹,
T. Montaruli⁶⁶, R. Morse⁴⁴, R. Nahnauer⁴¹, U. Naumann⁵⁶, G. Neer⁶⁹, H. Niederhausen⁸⁰,
S. C. Nowicki⁶⁴, D. R. Nygren⁵⁹, A. Obertacke Pollmann⁵⁶, A. Olivas⁵⁷, A. Omairat⁵⁶,
A. O’Murchadha⁴³, T. Palczewski⁸⁴, H. Pandya⁷⁰, D. V. Pankova⁴⁷, L. Paul⁴⁹, J. A. Pepper⁸⁴,
C. Pérez de los Heros⁶⁰, C. Pfendner⁵³, D. Pieloth⁶¹, E. Pinat⁴³, J. Posselt⁵⁶, P. B. Price⁵²,
G. T. Przybylski⁵⁹, J. Pütz⁴⁹, M. Quinnan⁴⁷, C. Raab⁴³, L. Rädcl⁴⁹, M. Rameez⁶⁶, K. Rawlins⁸⁵,
R. Reimann⁴⁹, M. Relich⁷⁴, E. Resconi⁴⁰, W. Rhode⁶¹, M. Richman⁸², S. Richter⁴⁴, B. Riedel⁶⁴,
S. Robertson³⁹, M. Rongen⁴⁹, C. Rott⁶², T. Ruhe⁶¹, D. Ryckbosch⁷¹, L. Sabbatini⁴⁴,
H.-G. Sander⁴⁸, A. Sandrock⁶¹, J. Sandroos⁴⁸, S. Sarkar^{76,86}, K. Schatto⁴⁸, F. Scheriau⁶¹,
M. Schimp⁴⁹, T. Schmidt⁵⁷, M. Schmitz⁶¹, S. Schoenen⁴⁹, S. Schöneberg⁵⁵, A. Schönwald⁴¹,
L. Schulte⁷⁷, L. Schumacher⁴⁹, D. Seckel⁷⁰, S. Seunarine⁸³, D. Soldin⁵⁶, M. Song⁵⁷,
G. M. Spiczak⁸³, C. Spiering⁴¹, M. Stahlberg⁴⁹, M. Stamatikos^{53,88}, T. Stanev⁷⁰, A. Stasik⁴¹,
A. Steuer⁴⁸, T. Stezelberger⁵⁹, R. G. Stokstad⁵⁹, A. Stöbl⁴¹, R. Ström⁶⁰, N. L. Strotjohann⁴¹,
G. W. Sullivan⁵⁷, M. Sutherland⁵³, H. Taavola⁶⁰, I. Taboada⁶⁵, J. Tatar^{59,52}, S. Ter-Antonyan⁷³,
A. Terliuk⁴¹, G. Tešić⁴⁷, S. Tilav⁷⁰, P. A. Toale⁸⁴, M. N. Tobin⁴⁴, S. Toscano⁶³, D. Tosi⁴⁴,
M. Tselengidou⁴⁶, A. Turcati⁴⁰, E. Unger⁶⁰, M. Usner⁴¹, S. Vallecorsa⁶⁶, J. Vandenbroucke⁴⁴,
N. van Eijndhoven⁶³, S. Vanheule⁷¹, J. van Santen⁴¹, J. Veenkamp⁴⁰, M. Vehring⁴⁹, M. Voge⁷⁷,
M. Vraeghe⁷¹, C. Walck⁴⁵, A. Wallace³⁹, M. Wallraff⁴⁹, N. Wandkowsky⁴⁴, Ch. Weaver⁶⁴,
C. Wendt⁴⁴, S. Westerhoff⁴⁴, B. J. Whelan³⁹, K. Wiebe⁴⁸, C. H. Wiebusch⁴⁹, L. Wille⁴⁴,
D. R. Williams⁸⁴, H. Wissing⁵⁷, M. Wolf⁴⁵, T. R. Wood⁶⁴, K. Woschnagg⁵², D. L. Xu⁴⁴,
X. W. Xu⁷³, Y. Xu⁸⁰, J. P. Yanez⁴¹, G. Yodh⁵¹, S. Yoshida⁷⁴, and M. Zoll⁴⁵

¹Institut d'Investigació per a la Gestió Integrada de les Zones Costaneres (IGIC) - Universitat Politècnica de València. C/ Paranimf 1 , 46730 Gandia, Spain.

²GRPHE - Université de Haute Alsace - Institut universitaire de technologie de Colmar, 34 rue du Grillenbreit BP 50568 - 68008 Colmar, France

³Technical University of Catalonia, Laboratory of Applied Bioacoustics, Rambla Exposició,08800 Vilanova i la Geltrú,Barcelona, Spain

⁴Friedrich-Alexander-Universität Erlangen-Nürnberg, Erlangen Centre for Astroparticle Physics, Erwin-Rommel-Str. 1, 91058 Erlangen, Germany

⁵Aix-Marseille Université, CNRS/IN2P3, CPPM UMR 7346, 13288 Marseille, France

⁶APC, Université Paris Diderot, CNRS/IN2P3, CEA/IRFU, Observatoire de Paris, Sorbonne Paris Cité, 75205 Paris, France

⁷IFIC - Instituto de Física Corpuscular, Edificios Investigación de Paterna, CSIC - Universitat de València, Apdo. de Correos 22085, 46071 Valencia, Spain

⁸LAM - Laboratoire d'Astrophysique de Marseille, Pôle de l'Étoile Site de Château-Gombert, rue Frédéric Joliot-Curie 38, 13388 Marseille Cedex 13, France

⁹INFN - Laboratori Nazionali del Sud (LNS), Via S. Sofia 62, 95123 Catania, Italy

¹⁰Nikhef, Science Park, Amsterdam, The Netherlands

¹¹Huygens-Kamerlingh Onnes Laboratorium, Universiteit Leiden, The Netherlands

¹²Universiteit van Amsterdam, Instituut voor Hoge-Energie Fysica, Science Park 105, 1098 XG Amsterdam, The Netherlands

¹³INFN -Sezione di Roma, P.le Aldo Moro 2, 00185 Roma, Italy

¹⁴Dipartimento di Fisica dell'Università La Sapienza, P.le Aldo Moro 2, 00185 Roma, Italy

¹⁵Institute for Space Science, RO-077125 Bucharest, Măgurele, Romania

¹⁶INFN - Sezione di Bologna, Viale Berti-Pichat 6/2, 40127 Bologna, Italy

¹⁷INFN - Sezione di Bari, Via E. Orabona 4, 70126 Bari, Italy

¹⁸Mediterranean Institute of Oceanography (MIO), Aix-Marseille University, 13288, Marseille, Cedex 9, France; Universit du Sud Toulon-Var, 83957, La Garde Cedex, France CNRS-INSU/IRD UM 110

¹⁹Géoazur, Université Nice Sophia-Antipolis, CNRS, IRD, Observatoire de la Côte d'Azur, Sophia Antipolis, France

²⁰Univ. Paris-Sud , 91405 Orsay Cedex, France

²¹Laboratoire de Physique Corpusculaire, Clermont Université, Université Blaise Pascal, CNRS/IN2P3, BP 10448, F-63000 Clermont-Ferrand, France

²²Institut für Theoretische Physik und Astrophysik, Universität Würzburg, Emil-Fischer Str. 31, 97074 Wrzburg, Germany

²³Dipartimento di Fisica e Astronomia dell'Università, Viale Berti Pichat 6/2, 40127 Bologna, Italy

²⁴INFN - Sezione di Catania, Viale Andrea Doria 6, 95125 Catania, Italy

²⁵Royal Netherlands Institute for Sea Research (NIOZ), Landsdiep 4,1797 SZ 't Horntje (Texel), The Netherlands

²⁶INFN - Sezione di Genova, Via Dodecaneso 33, 16146 Genova, Italy

-
- ²⁷Dipartimento di Fisica dell'Università, Via Dodecaneso 33, 16146 Genova, Italy
- ²⁸Universiteit Utrecht, Faculteit Betawetenschappen, Princetonplein 5, 3584 CC Utrecht, The Netherlands
- ²⁹Dr. Remeis-Sternwarte and ECAP, Universität Erlangen-Nürnberg, Sternwartstr. 7, 96049 Bamberg, Germany
- ³⁰Moscow State University, Skobeltsyn Institute of Nuclear Physics, Leninskie gory, 119991 Moscow, Russia
- ³¹Dipartimento di Fisica ed Astronomia dell'Università, Viale Andrea Doria 6, 95125 Catania, Italy
- ³²Direction des Sciences de la Matière - Institut de recherche sur les lois fondamentales de l'Univers - Service de Physique des Particules, CEA Saclay, 91191 Gif-sur-Yvette Cedex, France
- ³³INFN - Sezione di Pisa, Largo B. Pontecorvo 3, 56127 Pisa, Italy
- ³⁴Dipartimento di Fisica dell'Università, Largo B. Pontecorvo 3, 56127 Pisa, Italy
- ³⁵INFN -Sezione di Napoli, Via Cintia 80126 Napoli, Italy
- ³⁶University Mohammed I, Laboratory of Physics of Matter and Radiations, B.P.717, Oujda 6000, Morocco
- ³⁷Université de Strasbourg, IPHC, 23 rue du Loess 67037 Strasbourg, France - CNRS, UMR7178, 67037 Strasbourg, France
- ³⁸Dipartimento di Fisica dell'Università Federico II di Napoli, Via Cintia 80126, Napoli, Italy
- ³⁹Department of Physics, University of Adelaide, Adelaide, 5005, Australia
- ⁴⁰Technische Universität München, D-85748 Garching, Germany
- ⁴¹DESY, D-15735 Zeuthen, Germany
- ⁴²Dept. of Physics and Astronomy, University of Canterbury, Private Bag 4800, Christchurch, New Zealand
- ⁴³Université Libre de Bruxelles, Science Faculty CP230, B-1050 Brussels, Belgium
- ⁴⁴Dept. of Physics and Wisconsin IceCube Particle Astrophysics Center, University of Wisconsin, Madison, WI 53706, USA
- ⁴⁵Oskar Klein Centre and Dept. of Physics, Stockholm University, SE-10691 Stockholm, Sweden
- ⁴⁶Erlangen Centre for Astroparticle Physics, Friedrich-Alexander-Universität Erlangen-Nürnberg, D-91058 Erlangen, Germany
- ⁴⁷Dept. of Physics, Pennsylvania State University, University Park, PA 16802, USA
- ⁴⁸Institute of Physics, University of Mainz, Staudinger Weg 7, D-55099 Mainz, Germany
- ⁴⁹III. Physikalisches Institut, RWTH Aachen University, D-52056 Aachen, Germany
- ⁵⁰Physics Department, South Dakota School of Mines and Technology, Rapid City, SD 57701, USA
- ⁵¹Dept. of Physics and Astronomy, University of California, Irvine, CA 92697, USA
- ⁵²Dept. of Physics, University of California, Berkeley, CA 94720, USA
- ⁵³Dept. of Physics and Center for Cosmology and Astro-Particle Physics, Ohio State University, Columbus, OH 43210, USA
- ⁵⁴Dept. of Astronomy, Ohio State University, Columbus, OH 43210, USA
- ⁵⁵Fakultät für Physik & Astronomie, Ruhr-Universität Bochum, D-44780 Bochum, Germany
- ⁵⁶Dept. of Physics, University of Wuppertal, D-42119 Wuppertal, Germany

-
- ⁵⁷Dept. of Physics, University of Maryland, College Park, MD 20742, USA
- ⁵⁸Dept. of Physics and Astronomy, University of Kansas, Lawrence, KS 66045, USA
- ⁵⁹Lawrence Berkeley National Laboratory, Berkeley, CA 94720, USA
- ⁶⁰Dept. of Physics and Astronomy, Uppsala University, Box 516, S-75120 Uppsala, Sweden
- ⁶¹Dept. of Physics, TU Dortmund University, D-44221 Dortmund, Germany
- ⁶²Dept. of Physics, Sungkyunkwan University, Suwon 440-746, Korea
- ⁶³Vrije Universiteit Brussel, Dienst ELEM, B-1050 Brussels, Belgium
- ⁶⁴Dept. of Physics, University of Alberta, Edmonton, Alberta, Canada T6G 2E1
- ⁶⁵School of Physics and Center for Relativistic Astrophysics, Georgia Institute of Technology, Atlanta, GA 30332, USA
- ⁶⁶Département de physique nucléaire et corpusculaire, Université de Genève, CH-1211 Genève, Switzerland
- ⁶⁷Dept. of Physics, University of Toronto, Toronto, Ontario, Canada, M5S 1A7
- ⁶⁸Dept. of Astronomy and Astrophysics, Pennsylvania State University, University Park, PA 16802, USA
- ⁶⁹Dept. of Physics and Astronomy, Michigan State University, East Lansing, MI 48824, USA
- ⁷⁰Bartol Research Institute and Dept. of Physics and Astronomy, University of Delaware, Newark, DE 19716, USA
- ⁷¹Dept. of Physics and Astronomy, University of Gent, B-9000 Gent, Belgium
- ⁷²Institut für Physik, Humboldt-Universität zu Berlin, D-12489 Berlin, Germany
- ⁷³Dept. of Physics, Southern University, Baton Rouge, LA 70813, USA
- ⁷⁴Dept. of Physics, Chiba University, Chiba 263-8522, Japan
- ⁷⁵Dept. of Astronomy, University of Wisconsin, Madison, WI 53706, USA
- ⁷⁶Niels Bohr Institute, University of Copenhagen, DK-2100 Copenhagen, Denmark
- ⁷⁷Physikalisches Institut, Universität Bonn, Nussallee 12, D-53115 Bonn, Germany
- ⁷⁸CTSPS, Clark-Atlanta University, Atlanta, GA 30314, USA
- ⁷⁹Dept. of Physics, Yale University, New Haven, CT 06520, USA
- ⁸⁰Dept. of Physics and Astronomy, Stony Brook University, Stony Brook, NY 11794-3800, USA
- ⁸¹Université de Mons, 7000 Mons, Belgium
- ⁸²Dept. of Physics, Drexel University, 3141 Chestnut Street, Philadelphia, PA 19104, USA
- ⁸³Dept. of Physics, University of Wisconsin, River Falls, WI 54022, USA
- ⁸⁴Dept. of Physics and Astronomy, University of Alabama, Tuscaloosa, AL 35487, USA
- ⁸⁵Dept. of Physics and Astronomy, University of Alaska Anchorage, 3211 Providence Dr., Anchorage, AK 99508, USA
- ⁸⁶Dept. of Physics, University of Oxford, 1 Keble Road, Oxford OX1 3NP, UK
- ⁸⁷Earthquake Research Institute, University of Tokyo, Bunkyo, Tokyo 113-0032, Japan
- ⁸⁸NASA Goddard Space Flight Center, Greenbelt, MD 20771, USA

ABSTRACT

We present the results of searches for point-like sources of neutrinos based on the first combined analysis of data from both the ANTARES and IceCube neutrino telescopes. The combination of both detectors which differ in size and location forms a window in the Southern sky where the sensitivity to point sources improves by up to a factor of two compared to individual analyses. Using data recorded by ANTARES from 2007 to 2012, and by IceCube from 2008 to 2011, we search for sources of neutrino emission both across the Southern sky and from a pre-selected list of candidate objects. No significant excess over background has been found in these searches, and flux upper limits for the candidate sources are presented for $E^{-2.5}$ and E^{-2} power-law spectra with different energy cut-offs.

Subject headings: neutrino telescopes, neutrino astronomy, ANTARES, IceCube

1. Introduction

Neutrinos offer unique insight into the Universe due to the fact that they interact only weakly and via gravity. Unlike charged particles, they can travel straight from the source to the Earth without being deflected by magnetic fields or being absorbed. Neutrinos are expected to originate from the same locations where the acceleration of cosmic rays take place (Becker 2008; Gaisser et al. 1995; Halzen & Hooper 2002; Kelner & Aharonian 2008; Learned & Mannheim 2000; Murase 2015). A large variety of classes of astrophysical objects are predicted to be sources of high energy neutrinos, where galactic candidates include microquasars (Bednarek 2005; Levinson & Waxman 2001; Romero et al. 2003; Torres et al. 2005), supernova remnants (Alvarez-Muñiz & Halzen 2002; Cavasinni et al. 2006; González-García et al. 2014; Guetta & Amato 2003; Halzen et al. 2006; Mandelartz & Becker Tjus 2015; Vissani et al. 2011), or various objects close to the Galactic Center (Fujita et al. 2015; Kistler & Beacom 2006). Extragalactic sources comprise active galactic nuclei (Atoyan & Dermer 2001; Becker et al. 2005; Eichmann et al. 2012; Mannheim 1995; Mücke et al. 2003; Nellen et al. 1993; Rachen & Mészáros 1998; Stecker et al. 1991; Stecker 2005) and gamma ray bursts (Becker et al. 2006; Hümmer et al. 2012; Mészáros & Waxman 2001; Murase & Nagataki 2006; Razzaque et al. 2003; Waxman & Bahcall 1997, 2000).

The low neutrino cross section also implies that their detection is challenging. After the pioneering efforts by the Baikal (Aynutdinov et al. 2008) and AMANDA (Ahrens et al. 2002) collaborations, the field is presently led by the IceCube (Achterberg et al. 2006) and ANTARES (Ageron et al. 2011) experiments. IceCube, which is placed in the deep Antarctic ice, is the first detector to reach the cubic-kilometer size predicted to be necessary to detect cosmic neutrino fluxes according to the Waxman-Bahcall flux (Waxman & Bahcall 1999). Recently, IceCube has reported the crucial discovery of a flux of neutrinos up to \sim PeV energies which cannot be explained by

the background of atmospheric muons and neutrinos only (Aartsen et al. 2013c,b). The specific origin of these events is currently unknown. Some authors propose that at least part of the flux may have a galactic origin (Ahlers et al. 2015; Anchordoqui et al. 2014a,b; Bai et al. 2014; Fox et al. 2013; Padovani & Resconi 2014; Razzaque 2013), whereas others have focused on the extragalactic component (Cholis & Hooper 2013; Kalashev et al. 2013; Roulet et al. 2013; Stecker 2013). Meanwhile the ANTARES experiment has proven the feasibility of the Cherenkov telescope technique in sea water (Adrián-Martínez et al. 2012a, 2013b). While its instrumented volume is significantly smaller than that of IceCube, its geographical location provides a view of the Southern sky with significantly reduced background for neutrino energies below 100 TeV, and hence better sensitivity to many predicted Galactic sources of neutrinos in this part of the sky. The complementarity of the detectors with respect to Southern sky sources, due to their different geographical location, size and atmospheric muon background, allows for a gain in sensitivity by combining the analyses of data from both experiments in a joint search for point-like sources. The level of improvement depends on the details of the assumed astrophysical flux, in particular on its energy spectrum and the existence of a possible high-energy cut-off. The energy spectra are not yet known and predictions vary widely depending on the source model.

In this paper, a combined analysis using the point-source data samples of IceCube from 2008-2011 and of ANTARES from 2007-2012 is presented. This paper is structured as follows: in Section 2, the IceCube and ANTARES detectors are introduced. In Section 3 the samples from each experiment are described, while in Section 4 the search method is explained. Finally, the results are presented in Section 5 and the conclusions are discussed in Section 6.

2. The IceCube and ANTARES neutrino telescopes

IceCube is a cubic-kilometer neutrino telescope located at the geographic South Pole. It consists of a total of 5160 digital optical modules (DOMs) deployed in the Antarctic ice at depths from 1450 m to 2450 m below the surface (Abbasi et al. 2010). Each DOM consists of a pressure-resistant sphere that houses electronics, calibration LEDs, and a 10" PMT facing downward. The DOMs are configured in a hexagonal array of 86 vertical cables descending from the surface, called “strings”, with 60 DOMs per string. The average horizontal distance is 125 m between strings, and average vertical spacing is 17 m between DOMs on a string. A sub-array of eight strings (Deep Core) is also present in the core of the detector (Abbasi et al. 2012). These strings have a smaller separation in order to improve the sensitivity for lower energies. Construction of the detector began in 2005 and was completed six years later. The analysis presented in this paper is based on data from three years of the partially completed detector, when 40, 59, and 79 strings were deployed. Future joint analyses are envisioned that will be based on data from the full 86-string detector, including recent data samples that use outer detector modules as vetoes to achieve sensitivity to lower energy neutrinos.

ANTARES is the first neutrino telescope which operates in the sea (Ageron et al. 2011). It

was completed in 2008, with the first lines operating from 2006. It is located in the Mediterranean Sea at a depth of 2475 m, at coordinates (42° 48' N, 6° 10' E), 40 km South of Toulon (France). It consists of an array of 885 Optical Modules (OMs) distributed along 12 lines of 350 m height and an inter-line separation of 60 to 75 m. An OM consists of a 10" photomultiplier tube (PMT) contained inside a 17" glass sphere. The OMs are grouped into triplets and face downward at an angle of 45° in order to optimize the detection of up-going muon-neutrinos. There are 25 triplets (storeys) on each line, with a distance of about 15 m between storeys. Lines are kept vertical with a buoy at their top.

One of the main focuses of the ANTARES and IceCube neutrino telescopes is the observation of cosmic point-like sources of neutrino emission. At present, corresponding searches are mainly focused on the detection of muon neutrinos, which can be reconstructed with sub-degree angular resolution. Muon neutrinos are indirectly detected through the muon produced in their charged current interaction (CC) with a nucleus (N) inside or near to the detector volume:

$$\nu_\mu + N \rightarrow \mu^- + X \tag{1}$$

In this reaction, a muon and a hadronic shower, X, are produced.¹ The ultra-relativistic muon can travel long distances (up to several kilometers) and, when crossing a suitable medium such as ice or water, induce Cherenkov radiation that can be detected by the photomultipliers (PMTs) of neutrino telescopes. The corresponding charge and time information of the detected photons is used to reconstruct the direction of the muon, which is almost collinear with the original neutrino for energies above the TeV range. The main backgrounds for cosmic neutrino searches are atmospheric muons and neutrinos produced in the decay of the secondary particles created in the interactions of cosmic rays with the nuclei of the atmosphere.

3. Neutrino Data Samples

The data sample employed for this analysis corresponds to all events from the Southern sky which were included in the three-year IceCube point-source analysis (Aartsen et al. 2013d) combined with the events in the latest ANTARES point-source analysis (Adrián-Martínez et al. 2014). The ANTARES sample contains data recorded from Jan 29, 2007 to Dec 31, 2012; for IceCube the data was recorded from Apr 5, 2008 to May 13, 2011 with the partially completed detector, and without the use of the Deep Core strings.

Detector performance differs not only between ANTARES and IceCube, but also between the three IceCube configurations as the detector grew, from 40, to 59, and then to 79 strings. The

¹In this work the charge conjugate particles and reactions will be implicitly included, i.e. in this case the reaction $\bar{\nu}_\mu + N \rightarrow \mu^+ + X$ is also assumed.

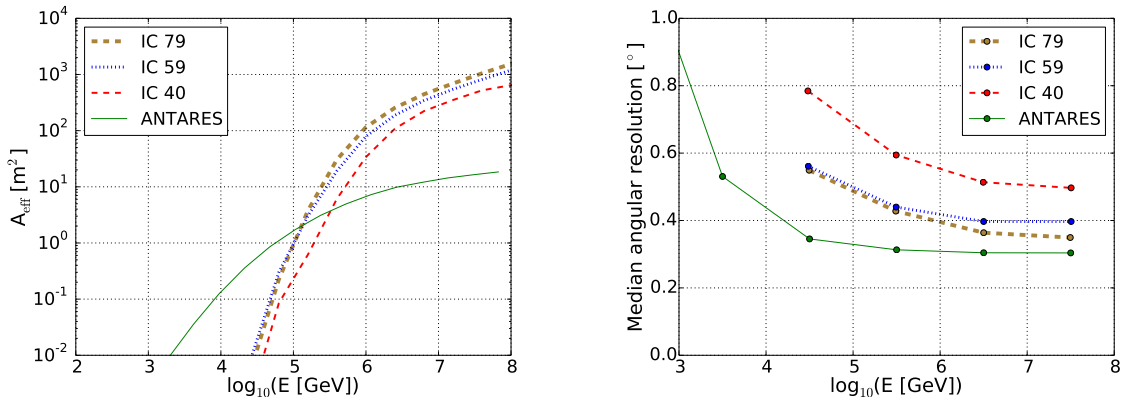


Fig. 1.— Muon neutrino effective area for a point source at a declination $\delta = -30^\circ$ (left) and median angular resolution (right) for the samples used in this analysis after the final set of cuts. The median angular resolution is defined as the median of the difference between the true neutrino direction and the reconstructed muon direction.

effective area is defined as the equivalent surface with a perfect efficiency which detects the same number of events as the detector. For a source position of $\delta = -30^\circ$, the effective area for each IceCube configuration and for ANTARES is shown in Figure 1-left. Due to its larger size, the effective area for the IceCube samples is larger for neutrino energies above ~ 100 TeV. However, to view sources in the Southern Sky, IceCube must contend with the down-going background of atmospheric muons, which becomes overwhelming at lower energies. To minimize these, the IceCube point-source analysis introduced a declination-dependent energy cut which strongly suppresses low energy events in the final data sample. ANTARES, which can use the Earth as a filter against atmospheric muons in the Southern sky, thus maintains a larger effective area in this energy and declination range.

A comparison of the median angular resolution of each sample can be seen in Figure 1-right. The better resolution of the ANTARES sample is due to the longer photon scattering length in water compared to ice. The sensitivities reported by both experiments for the whole sky using the Neyman method (Neyman 1937) are shown in Figure 2.

Different selection criteria are applied to each sample. A summary of these selections, which in all cases were developed with a data blinding policy and were optimised to minimise the neutrino flux needed for a 5σ discovery in 50% of the experiments, is given below.

3.1. ANTARES

The ANTARES data sample used for this analysis corresponds to the events coming from the Southern Sky used in the last published point source analysis (Adrián-Martínez et al. 2014).

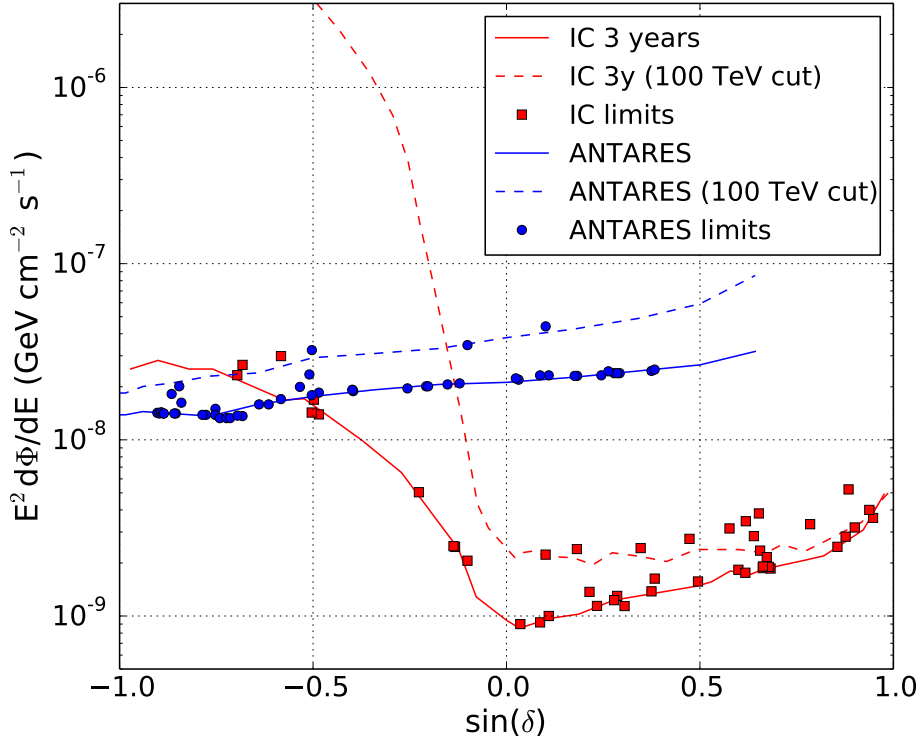


Fig. 2.— 90% CL limits for selected sources (squares and dots) and sensitivities using the Neyman method as a function of the declination (lines) reported in the ANTARES 2007-2012 (blue) (Adrián-Martínez et al. 2014) and the IceCube 3 years (red) (Aartsen et al. 2013d) point source analyses. An unbroken E^{-2} power-law source spectrum is assumed for the limits and lower sensitivity curves (solid lines). Dashed lines indicate the sensitivity for an E^{-2} spectrum with neutrino energies of $E_\nu \leq 100$ TeV using the Neyman method.

The parameters which are used to optimise this sample are the quality of the track fit, Λ , the angular error estimate, σ (also denoted as β in most ANTARES publications), and the zenith angle, θ . These three parameters are given by the track reconstruction of neutrino events, which uses a maximum likelihood (ML) method (Adrián-Martínez et al. 2012b, 2013a). The algorithm is based on a multi-step procedure to fit the direction of the reconstructed muon by maximising the Λ parameter. The angular error estimate, σ , is obtained from the uncertainty on the zenith and azimuth angles extracted from the covariance matrix.

The selection yields a total of 5516 events for the whole sky, with 4136 of these events in the Southern Hemisphere. The estimated contamination of mis-reconstructed atmospheric muons is 10%.

3.2. IceCube

The IceCube data samples used for this analysis are based on the event selection optimized for point source searches with the data recorded using the 40, 59, and 79-string detector configurations, summarized in Table 1. Only events from the Southern sky are selected here for the joint analysis. In contrast to the ANTARES selection above, IceCube’s Southern sky events are predominantly atmospheric muons rather than atmospheric neutrinos, because the Earth cannot be used as a neutrino filter for directions above the detector.

The total number of down-going events in IceCube is $\sim 10^{10}$ per year. The down-going events that were selected as part of the above analyses and which are used here comprise only well-reconstructed muon tracks at very high energies, where it becomes possible to detect a neutrino source with a hard E^{-2} energy spectrum beyond the more steeply falling atmospheric muon background, and from clustering of events in a single region of the sky. For the 40 string configuration, a set of cuts on the reduced log-likelihood of the track reconstruction, the angular uncertainty, σ , and the muon energy proxy is performed for events coming from the Southern Sky (Abbasi et al. 2011). For the 59 string configuration, the vetoing capability of IceTop is added to reduce the background of atmospheric muons (Aartsen et al. 2013d). For the 79 string configuration, the event selection is performed based on boosted decision trees using 17 observables, and includes the use of the IceTop veto.

The total number of Southern sky events selected from the three year sample is 146 018 events.

3.3. Relative fraction of source events for different source assumptions

The relative fraction of expected source events from each sample needs to be calculated in order to estimate its respective weight in the likelihood which will be used to search for an excess of events from a particular direction (see Section 4). This fraction is defined as the ratio of the expected number of signal events for the given sample to that for all samples,

Table 1. Event samples for the different IceCube detector configurations, labelled by the number of strings deployed. Only Southern-sky events (numbers indicated by last column) have been selected for the present analysis.

Sample	Start date	End date	Livetime [days]	# events
IC-40	2008 Apr 5	2009 May 20	376	22 779
IC-59	2009 May 20	2010 May 31	348	64 230
IC-79	2010 May 31	2011 May 13	316	59 009

$$C^j(\delta, d\Phi/dE_\nu) = \frac{N^j(\delta, d\Phi/dE_\nu)}{\sum_i N^i(\delta, d\Phi/dE_\nu)}, \quad (2)$$

where the total number of expected events for the j -th sample, N^j , with a given source declination, δ , and a given source spectrum, $\frac{d\Phi}{dE_\nu}$, can be calculated as

$$N^j\left(\delta, \frac{d\Phi}{dE_\nu}\right) = \int dt \int dE_\nu A_{\text{eff}}^j(E_\nu, \delta) \frac{d\Phi}{dE_\nu}. \quad (3)$$

The time integration extends over the live time of each sample and $A_{\text{eff}}^j(E_\nu, \delta)$ indicates the effective area of the corresponding detector layout j as a function of the neutrino energy, E_ν , and the declination of the source, δ .

Since each detector layout has a different response depending on the neutrino energy and declination, this relative fraction of source events needs to be calculated for different source spectra and source declinations. Figure 3 shows the relative fraction of signal events for an unbroken E^{-2} spectrum, which corresponds to vanilla first order Fermi acceleration (Bandford & Ostriker 1978; Krymskii 1997). In this case, there is a significant contribution from all samples over most of the Southern Sky, with the ANTARES contribution being more significant for declinations closer to $\delta = -90^\circ$, and IceCube for declinations closer to 0° . The reason for this variability is mostly due to the declination-dependent energy cut applied in the IceCube samples to reduce the background of atmospheric muons.

Other source assumptions are also considered in this analysis. The relative fraction of source events is calculated for an unbroken $E^{-2.5}$ power-law spectrum, as suggested in recent IceCube diffuse-flux searches (Aartsen et al. 2015), and for an E^{-2} spectrum with exponential square-root cut-offs ($\frac{d\Phi}{dE} \propto E^{-2} \exp\left[-\sqrt{\frac{E}{E_{\text{cut-off}}}}\right]$) of 100 TeV, 300 TeV and 1 PeV, since a square-root dependence may be expected from Galactic sources (Kappes et al. 2007). Figure 4 shows the relative fraction of source events for these cases. Compared with an unbroken E^{-2} spectrum, the contribution of high energy neutrinos in all of these cases is lower, and therefore the relative contribution of the ANTARES sample increases.

4. Search method

An unbinned maximum likelihood ratio estimation has been performed to search for excesses of events that would indicate cosmic neutrinos coming from a common source. In order to estimate the significance of a cluster of events, this likelihood takes into account the energy and directional information of each event. Due to the different detector response, the data sample which an event belongs to is also taken into account. The likelihood, as a function of the total number of fitted signal events, n_s , can be expressed as:

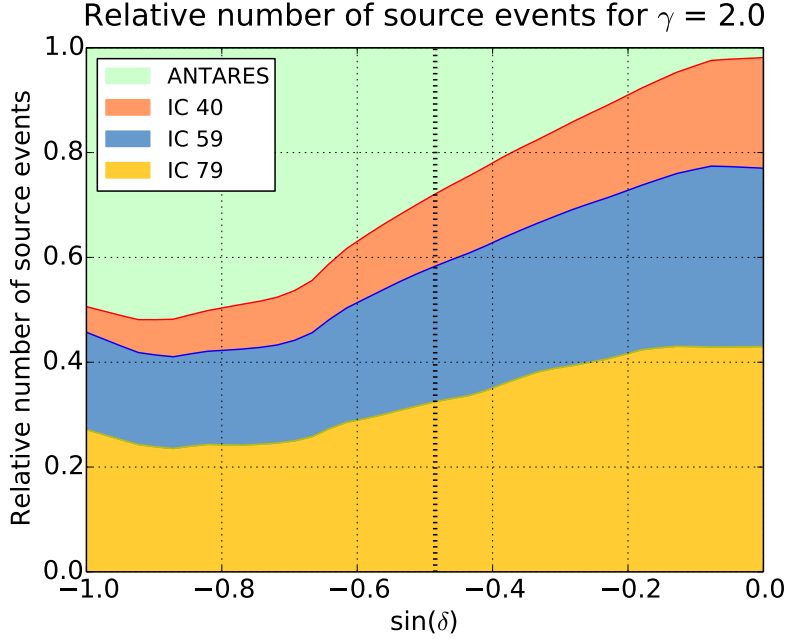


Fig. 3.— Relative fraction of signal events for each sample as a function of the source declination for the case of an E^{-2} energy spectrum. The orange, blue, and yellow shaded areas correspond to the IceCube 40, 59 and 79-string data samples, respectively, and the green shaded area indicates the ANTARES 2007-2012 sample. The vertical dashed line marks the declination of the Galactic Center.

$$L(n_s) = \prod_{j=1}^4 \prod_{i=1}^{N^j} \left[\frac{n_s^j}{N^j} S_i^j + \left(1 - \frac{n_s^j}{N^j} \right) B_i^j \right] \quad (4)$$

where j marks one of the four data samples, i indicates an event belonging to the j -th sample, S_i^j is the value of the signal probability distribution function (PDF) for the i -th event, B_i^j indicates the value of the background PDF, N^j is the total number of events in the j -th sample, and n_s^j is the number of signal events fitted for in the j -th sample. Since a given evaluation of the likelihood refers to a single source hypothesis at a fixed sky location, the number of signal events n_s^j that is fitted for in each sample is related to the total number of signal events n_s by the relative contribution of each sample, $n_s^j = n_s \cdot C^j(\delta, \frac{d\Phi}{dE})$.

The signal and background PDFs for the IceCube and ANTARES samples have slightly different definitions. The signal PDF for ANTARES is defined as

$$S^{ANT} = \frac{1}{2\pi\sigma^2} \exp\left(-\frac{\Delta\Psi(\vec{x}_s)^2}{2\sigma^2}\right) P_s^{ANT}(\mathcal{N}^{hits}, \sigma), \quad (5)$$

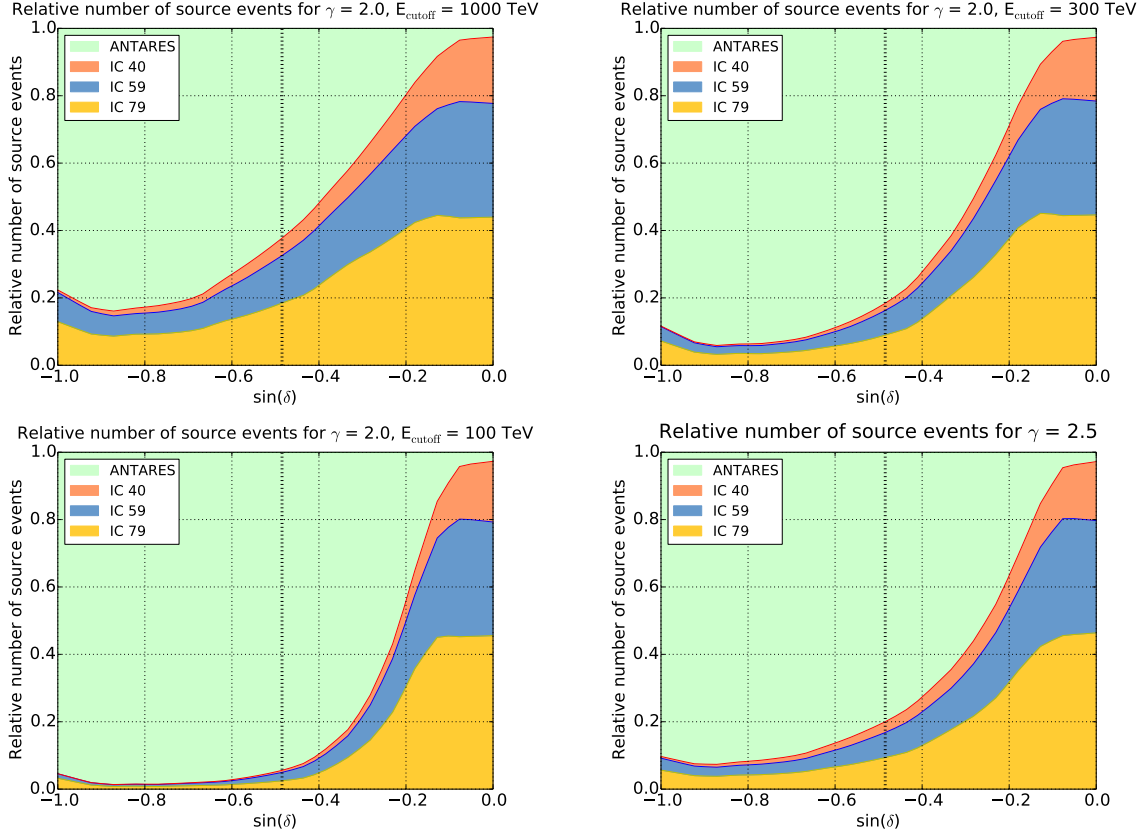


Fig. 4.— Relative fraction of signal events of each sample as a function of the source declination for different energy spectra: E^{-2} with energy cutoff E_{cutoff} of 1 PeV (top-left), 300 TeV (top-right), 100 TeV (bottom-left); and $E^{-2.5}$ spectrum (bottom-right). The orange, blue and yellow shaded areas correspond to the IceCube 40, 59 and 79-string data samples, respectively, and the green shaded area indicates the ANTARES 2007-2012 sample. The vertical dashed line corresponds to the declination of the Galactic Center.

where $\vec{x}_s = (\alpha_s, \delta_s)$ indicates the source direction in equatorial coordinates, $\Delta\Psi(\vec{x}_s)$ is the angular distance of a given event to the source and $P_s^{ANT}(\mathcal{N}^{\text{hits}}, \sigma)$ is the probability for a signal event to be reconstructed with an angular error estimate of σ and a number of hits $\mathcal{N}^{\text{hits}}$. The number of hits is a proxy for the energy of the event. In this sense, an event with a higher number of hits (higher deposited energy) would be less likely to be produced by the expected background.

The definition of the signal PDFs for the IceCube samples is similar,

$$S^{IC} = \frac{1}{2\pi\sigma^2} \exp\left(-\frac{\Delta\Psi(\vec{x}_s)^2}{2\sigma^2}\right) P_s^{IC}(\mathcal{E}, \sigma|\delta) \quad (6)$$

where the main difference lies in the use of the reconstructed energy, \mathcal{E} , and the declination depen-

dence of the probability for a signal event to be reconstructed with a given σ and \mathcal{E} . The declination dependence is needed mainly because of the event selection cut on reconstructed energy, which is designed to reduce the atmospheric muon background.

Background events are expected to be distributed uniformly in right ascension. The background PDFs are in fact obtained from the experimental data itself. The definition of the PDFs are:

$$B^{ANT} = \frac{B^{ANT}(\delta)}{2\pi} P_b^{ANT}(\mathcal{N}^{hits}, \sigma), \quad (7)$$

$$B^{IC} = \frac{B^{IC}(\delta)}{2\pi} P_b^{IC}(\mathcal{E}, \sigma|\delta), \quad (8)$$

where $B^j(\delta)$ is the per-solid-angle rate of observed events as a function of the declination in the corresponding sample. $P_b^{ANT}(\mathcal{N}^{hits}, \sigma)$ and $P_b^{IC}(\mathcal{E}, \sigma|\delta)$ characterize the distributions for background event properties, in analogy with the definitions of P_s^{ANT} and P_s^{IC} for signal events given above.

The test statistic, TS, is determined from the likelihood (Eq. 4) as $TS = \log L(\hat{n}_s) - \log L(n_s = 0)$, where \hat{n}_s is the value that maximizes the likelihood. The larger the TS, the lower the probability (p-value) of the observation to be produced by the expected background. Simulations are performed to obtain the distributions of the TS. The significance (specifically, the p-value) of an observation is determined by the fraction of TS values which are larger than the observed TS.

The TS is calculated as a preliminary step to obtain the post-trial p-values of a search. TS distributions for the fixed-source, background-only hypothesis have been calculated in steps of 1° in declination from pseudo-data sets of randomized data. Because these distributions vary with declination, the preliminary TS is turned into a “pre-trial p-value” by comparing the TS obtained at the source location from the data to the background TS distribution for the corresponding declination. The post-trial significance is then estimated with pseudo-data sets and according to the type of search, as explained together with the results in Section 5.

Two different searches for point-like neutrino sources have been performed. In the candidate list search, a possible excess of neutrino events is looked for at the location of 40 pre-selected neutrino source candidates. Since the location of these sources is fixed (at known locations with an uncertainty below the angular resolution of all samples) only the number of signal events n_s is a free parameter in the likelihood maximisation. These candidates correspond to all sources in the Southern sky considered in the previous candidate-source list searches performed in the ANTARES and IceCube point-source analyses (Aartsen et al. 2013d; Adrián-Martínez et al. 2014).

The second search is a “full sky” search, looking for a significant point-like excess anywhere in the Southern sky. For this purpose, the likelihood is evaluated in steps of $1^\circ \times 1^\circ$ over the whole scanned region. In this case, the source position is an additional free parameter of the likelihood to fit the best position within the $1^\circ \times 1^\circ$ boundaries.

Both the full Southern-sky and candidate-list searches have been performed using an E^{-2} source spectrum in the signal PDFs. The main virtue of the energy term in the PDFs is to add power to distinguish signal neutrinos from the softer spectra of atmospheric neutrinos and atmospheric muons. Limits for the sources in the candidate list have also been calculated for the source spectra mentioned in Section 3.3.

5. Results

Results from the full Southern sky and candidate list searches are detailed below.

5.1. Full Southern-sky search

No significant event clusters are found over the expected background. The most significant cluster is located at equatorial coordinates $\alpha = 332.8^\circ$, $\delta = -46.1^\circ$, with best-fit $n_s = 7.9$ and pre-trial p-value of 6.0×10^{-7} . Figure 5 shows this pre-trial p-value compared to the distribution of smallest p-values found when performing the same analysis on many pseudo-data sets (constructed by randomizing the right ascension coordinates of the real data). It is found that 24% of pseudo-data sets have a smaller p-value somewhere in the sky than is found in the real data; the post-trial significance is thus 24% (0.7σ in the one-sided sigma convention). The direction of this cluster is consistent with, but also less significant than the second most significant cluster in the previous ANTARES point-source analysis. Figure 6 shows the position of this cluster and the pre-trial p-values for all directions in the Southern sky (a smaller step of $0.2^\circ \times 0.2^\circ$ is used to plot this map).

5.2. Candidate list search

The results of the candidate source list search are presented in Table 2. No statistically significant excess is found. The most significant excess for any object on the list corresponds to HESS J1741-302 with a pre-trial p-value of 0.003. To account for trial factors, the search is performed on the same list of sources using pseudo data-sets, and the distribution of smallest p-values for these searches is shown in Figure 7. We find that 11% of randomized data sets have a smaller p-value for any source than that found for the real data; the post-trial significance of the source list search is thus 11% (1.2σ in the one-sided sigma convention).

Table 2 provides the pre-trial p-values, best-fit signal events n_s and flux upper limits (under different assumptions of the energy spectrum) for all the candidate source objects. Figure 8 shows the Neyman sensitivities and limits for this search (assuming an E^{-2} spectrum) in comparison with the previously published ANTARES and IceCube analyses of the same data. The point-source sensitivity in a substantial region of the sky, centered approximately at the declination of the

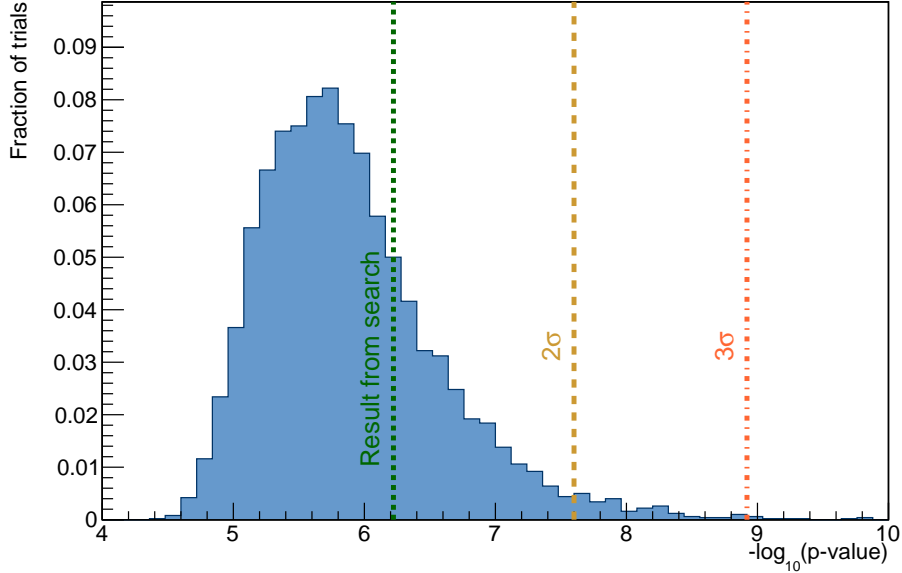


Fig. 5.— Distribution of the smallest p-value in the Southern sky obtained from scans of pseudo-data sets. Green line: pre-trial p-value for the most significant source location found. Yellow and red lines: pre-trial p-values for the 2σ and 3σ significance thresholds using the one-sided sigma convention.

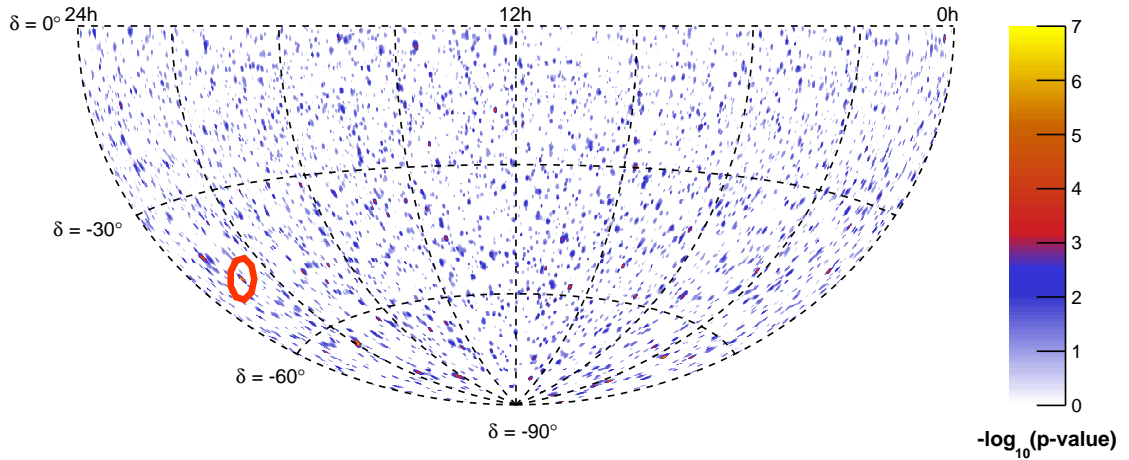


Fig. 6.— Skymap of pre-trial p-values for the combined ANTARES 2007-2012 and IceCube 40, 59, 79 point-source analyses. The red circle indicates the location of the most significant cluster (0.7σ post-trial significance in the one-sided sigma convention), discussed in the text.

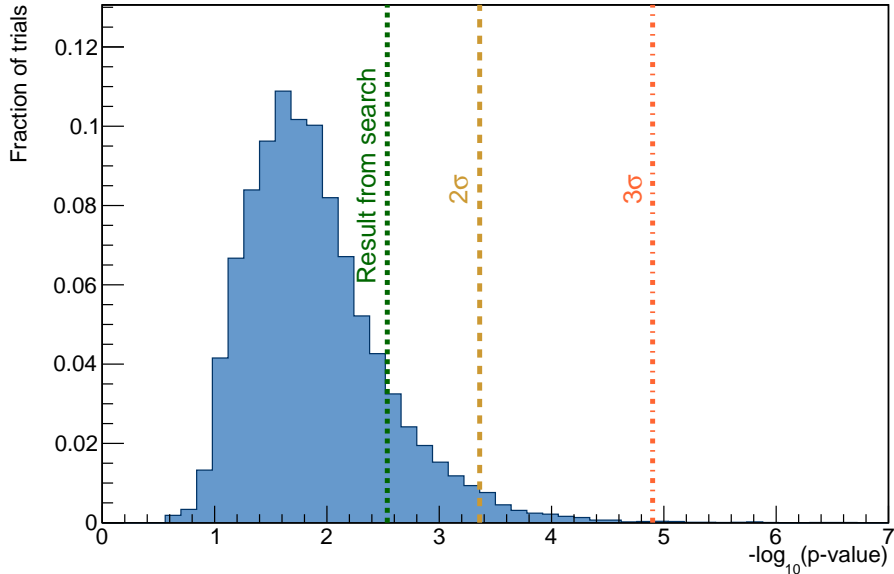


Fig. 7.— Distribution of the smallest p-value found in each candidate-list analysis of a pseudo-data set. Green line: pre-trial p-value for the most significant object found in the real data. Yellow and red lines: pre-trial p-values needed for the 2 and 3 σ post-trial significance thresholds in the one-sigma convention.

Galactic center ($\delta = -29^\circ$), can be seen to have improved by up to a factor of two. A maximum gain of at most $\sqrt{2}$ would be expected in a background-dominated sample; however, the low number of effective background events (with reconstructed energy and direction mimicking an astrophysical neutrino) is very low, so that gains of more than $\sqrt{2}$ are possible. Similar gains in other regions of the sky can be seen for different energy spectra in Figure 9.

6. Conclusion

We have presented the first combined point-source analysis of data from the ANTARES and IceCube detectors. Their different characteristics, in particular IceCube’s larger size and ANTARES’ location in the Northern hemisphere, complement each other for Southern sky searches. We have calculated the sensitivity to point sources and, with respect to an analysis of either data set alone, found that up to a factor of two improvement is achieved in different regions of the Southern sky, depending on the energy spectrum of the source. Two joint analyses of the data sets have been performed: a search over the whole Southern sky for a point-like excess of neutrino events, and a targeted analysis of 40 pre-selected candidate source objects. The largest excess in the Southern sky

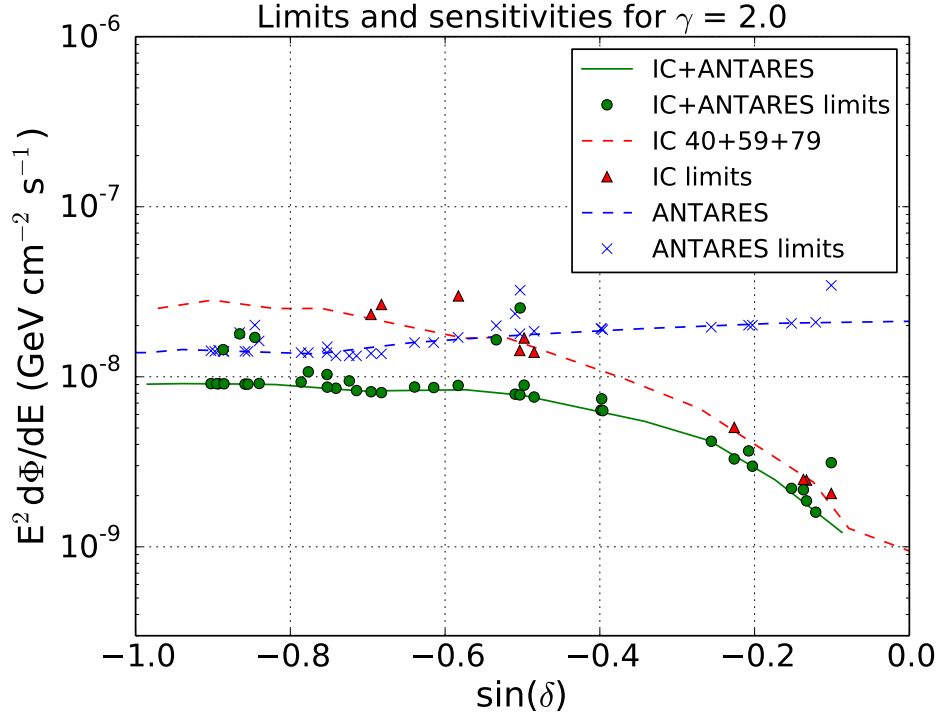


Fig. 8.— 90% CL sensitivities and limits (Neyman method) for the neutrino emission from point sources as a function of source declination in the sky, for an assumed E^{-2} energy spectrum of the source. Green points indicate the actual limits on the candidate sources. The green line indicates the sensitivity of the combined search. Curves/points respectively indicate the published sensitivities/limits for the IceCube (blue) and ANTARES (red) analyses, respectively. As reference, the declination of the Galactic Center is approximately at $\sin(\delta = -29^\circ) \approx -0.48$.

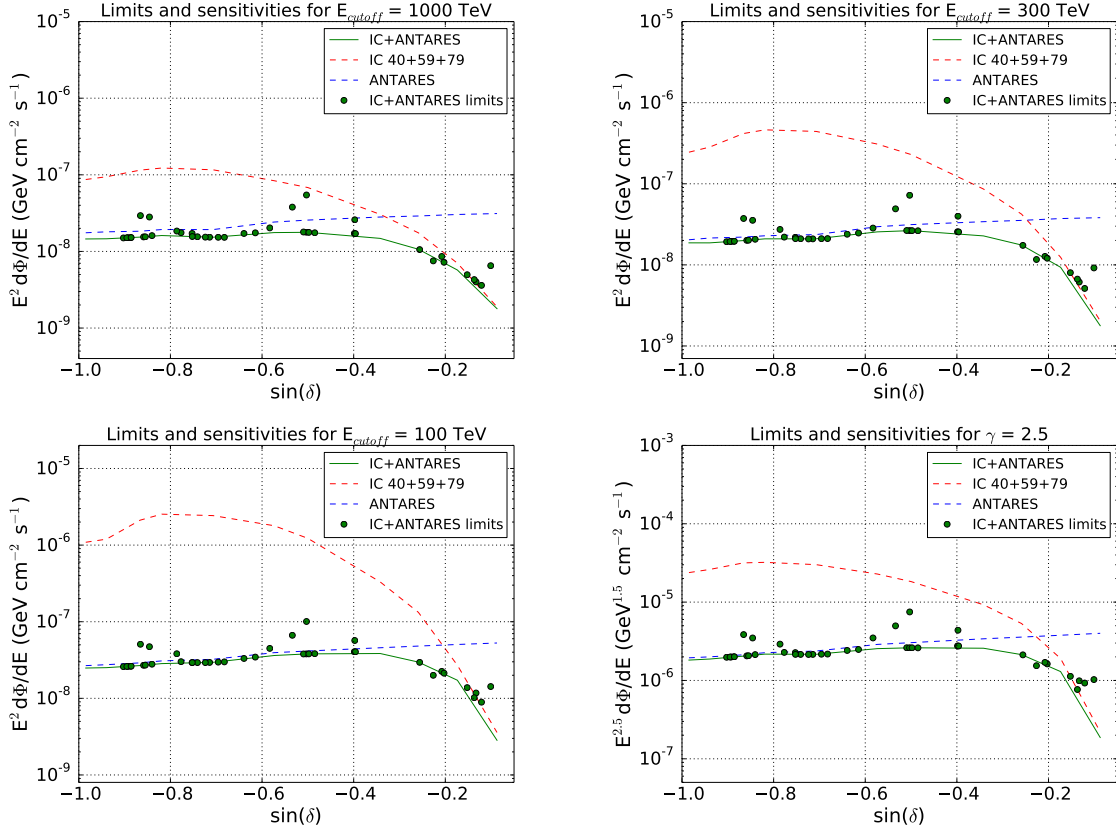


Fig. 9.— Point source sensitivities and limits as in Fig. 8, for other energy spectra: E^{-2} with a square-root exponential cut-off at $E = 1 \text{ PeV}$ (top left), $E = 300 \text{ TeV}$ (top right), $E = 100 \text{ TeV}$ (bottom left) and $E^{-2.5}$ unbroken power-law (bottom right). Green points indicate the actual limits on the candidate sources. The green line indicates the sensitivity for the combined search. Red and blue curves indicate the sensitivities for the individual IceCube and ANTARES analyses, respectively. As reference, the declination of the Galactic Center is approximately at $\sin(\delta = -29^\circ) \approx -0.48$.

Table 2. Fitted number of source events, n_s , pre-trial p-values, p , and 90% C.L. flux limits, Φ_ν^{90CL} for the different source spectra for the 40 candidate sources. Units for the flux limits for the $E^{-2.5}$ spectra, $\phi_{E^{-2.5}}^{90CL}$, are given in $\text{GeV}^{1.5}\text{cm}^{-2}\text{s}^{-1}$, whereas the rest are in $\text{GeV cm}^{-2}\text{s}^{-1}$. The sources are sorted by their declination. Dashes (-) in the fitted number of source events and pre-trial p-values indicate sources with $n_s \leq 0.001$.

Name	δ ($^\circ$)	α ($^\circ$)	n_s	p	$\phi_{E^{-2}}^{90CL}$	$\phi_{E_c=1PeV}^{90CL}$	$\phi_{E_c=300TeV}^{90CL}$	$\phi_{E_c=100TeV}^{90CL}$	$\phi_{E^{-2.5}}^{90CL}$
3C279	-5.8	-166.0	1.1	0.05	3.1E-09	1.0E-06	6.5E-09	9.2E-09	6.7E-08
HESSJ1837-069	-7.0	-80.6	-	-	1.6E-09	9.3E-07	1.5E-08	2.0E-08	2.6E-08
QSO2022-077	-7.6	-53.6	-	-	1.9E-09	1.7E-06	1.7E-08	2.5E-08	3.5E-08
PKS1406-076	-7.9	-147.8	-	-	2.2E-09	7.7E-07	4.3E-09	6.7E-09	1.0E-08
HESSJ1834-087	-8.8	-81.3	-	-	2.2E-09	1.1E-06	1.6E-08	2.1E-08	2.9E-08
PKS0727-11	-11.7	112.6	-	-	3.0E-09	9.9E-07	1.5E-08	5.1E-09	8.9E-09
1ES0347-121	-12.0	57.4	-	-	3.7E-09	2.5E-06	1.8E-08	2.6E-08	3.8E-08
QSO1730-130	-13.1	-96.7	-	-	3.3E-09	2.3E-06	1.8E-08	2.6E-08	3.8E-08
LS5039	-14.8	-83.4	-	-	4.2E-09	2.1E-06	1.1E-08	1.7E-08	2.9E-08
W28	-23.3	-89.6	-	-	6.3E-09	2.8E-06	1.7E-08	2.5E-08	4.0E-08
PKS0454-234	-23.4	74.3	-	-	7.4E-09	2.2E-06	2.6E-08	2.7E-08	3.8E-08
1ES1101-232	-23.5	165.9	-	-	6.4E-09	2.6E-06	7.2E-09	1.2E-08	2.1E-08
Galactic Center	-29.0	-93.6	-	-	7.6E-09	2.6E-06	1.8E-08	2.6E-08	3.8E-08
PKS1622-297	-29.9	-113.5	-	-	8.9E-09	2.6E-06	1.7E-08	2.2E-08	2.9E-08
HESSJ1741-302	-30.2	-94.8	1.6	0.003	2.5E-08	7.5E-06	5.5E-08	7.2E-08	1.0E-07
PKS2155.304	-30.2	-30.3	-	-	7.8E-09	2.6E-06	2.0E-08	2.8E-08	4.5E-08
H2356-309	-30.6	-8.2	-	-	7.9E-09	1.5E-06	1.5E-08	2.1E-08	3.0E-08
PKS0548-322	-32.3	87.7	0.9	0.07	1.6E-08	5.0E-06	3.8E-08	4.9E-08	1.4E-08
PKS1454-354	-35.7	-135.6	-	-	8.9E-09	3.5E-06	8.6E-09	2.1E-08	3.0E-08
PKS0426-380	-37.9	67.2	-	-	8.6E-09	2.8E-06	7.5E-09	1.2E-08	2.0E-08
RXJ1713.7-3946	-39.8	-101.8	-	-	8.7E-09	2.0E-06	1.5E-08	2.0E-08	2.6E-08
CenA	-43.0	-158.6	-	-	8.1E-09	2.2E-06	4.0E-09	6.1E-09	1.2E-08
PKS0537-441	-44.1	84.7	-	-	8.2E-09	1.6E-06	1.8E-08	2.6E-08	4.1E-08
VelaX	-45.6	128.8	-	-	8.3E-09	2.2E-06	1.5E-08	2.1E-08	2.9E-08
RXJ0852.0-4622	-46.4	133.0	-	-	9.5E-09	2.1E-06	1.5E-08	2.1E-08	2.9E-08
HESSJ1632-478	-47.8	-112.0	-	-	8.6E-09	2.1E-06	1.6E-08	2.1E-08	2.9E-08
PKS2005-489	-48.8	-57.6	-	-	1.0E-08	2.9E-06	1.7E-08	1.3E-08	2.2E-08
GX339-4	-48.8	-104.3	-	-	8.7E-09	2.2E-06	1.6E-08	2.1E-08	2.8E-08
HESSJ1616-508	-51.0	-116.0	-	-	1.1E-08	2.3E-06	1.8E-08	2.2E-08	3.0E-08
HESSJ1614-518	-51.8	-116.4	-	-	9.3E-09	2.1E-06	1.6E-08	2.0E-08	2.7E-08
CirX-1	-57.2	-129.8	-	-	9.1E-09	2.1E-06	1.8E-08	2.7E-08	3.8E-08
HESSJ1023-575	-57.8	155.8	0.8	0.08	1.7E-08	3.5E-06	2.8E-08	3.5E-08	4.7E-08
HESSJ1503-582	-58.7	-133.6	-	-	9.1E-09	2.0E-06	1.5E-08	1.9E-08	2.6E-08
MSH15-52	-59.2	-131.5	-	-	9.1E-09	2.1E-06	1.5E-08	2.0E-08	2.7E-08
ESO139-G12	-59.9	-95.6	0.8	0.07	1.8E-08	3.9E-06	2.9E-08	3.7E-08	5.1E-08
HESSJ1507-622	-62.3	-133.3	-	-	9.1E-09	2.0E-06	5.0E-09	8.0E-09	1.4E-08
RCW86	-62.5	-139.3	0.2	0.11	1.4E-08	4.4E-06	3.6E-09	4.0E-08	5.7E-08
HESSJ1303-631	-63.2	-164.2	-	-	9.1E-09	2.0E-06	1.5E-08	1.9E-08	2.6E-08
PSRB1259-63	-63.5	-164.3	-	-	9.1E-09	2.4E-06	1.7E-08	2.4E-08	3.3E-08
HESSJ1356-645	-64.5	-151.0	-	-	9.1E-09	2.0E-06	1.5E-08	1.9E-08	2.6E-08

search has a post-trial probability of 24% (significance of 0.7σ), located at $\alpha = 332.8^\circ$, $\delta = -46.1^\circ$ in equatorial coordinates. In the source list search, the candidate with the highest significance corresponds to HESS J1741-302, with a post-trial probability of 11% (significance of 1.2σ). Both of the results are compatible with the background-only hypothesis. Flux upper limits for each of the source candidates have been calculated for E^{-2} and $E^{-2.5}$ power-law energy spectra, as well as for E^{-2} spectra with cut-offs at energies of 1 PeV, 300 TeV, and 100 TeV. Because of their complementary nature, with IceCube providing more sensitivity at higher energies and ANTARES at lower energies, a joint analysis of future data sets will continue to provide the best point-source sensitivity in critical overlap regions in the Southern sky, where neutrino emission from Galactic sources in particular may be found.

The authors of the ANTARES collaboration acknowledge the financial support of the funding agencies: Centre National de la Recherche Scientifique (CNRS), Commissariat à l'énergie atomique et aux énergies alternatives (CEA), Commission Européenne (FEDER fund and Marie Curie Program), Région Île-de-France (DIM-ACAV) Région Alsace (contrat CPER), Région Provence-Alpes-Côte d'Azur, Département du Var and Ville de La Seyne-sur-Mer, France; Bundesministerium für Bildung und Forschung (BMBF), Germany; Istituto Nazionale di Fisica Nucleare (INFN), Italy; Stichting voor Fundamenteel Onderzoek der Materie (FOM), Nederlandse organisatie voor Wetenschappelijk Onderzoek (NWO), the Netherlands; Council of the President of the Russian Federation for young scientists and leading scientific schools supporting grants, Russia; National Authority for Scientific Research (ANCS), Romania; Ministerio de Economía y Competitividad (MINECO), Prometeo and Grisolia programs of Generalitat Valenciana and MultiDark, Spain; Agence de l'Oriental and CNRST, Morocco. We also acknowledge the technical support of Ifremer, AIM and Foselev Marine for the sea operation and the CC-IN2P3 for the computing facilities.

The authors of the IceCube collaboration acknowledge the support from the following agencies: U.S. National Science Foundation-Office of Polar Programs, U.S. National Science Foundation-Physics Division, University of Wisconsin Alumni Research Foundation, the Grid Laboratory Of Wisconsin (GLOW) grid infrastructure at the University of Wisconsin - Madison, the Open Science Grid (OSG) grid infrastructure; U.S. Department of Energy, and National Energy Research Scientific Computing Center, the Louisiana Optical Network Initiative (LONI) grid computing resources; Natural Sciences and Engineering Research Council of Canada, WestGrid and Compute/Calcul Canada; Swedish Research Council, Swedish Polar Research Secretariat, Swedish National Infrastructure for Computing (SNIC), and Knut and Alice Wallenberg Foundation, Sweden; German Ministry for Education and Research (BMBF), Deutsche Forschungsgemeinschaft (DFG), Helmholtz Alliance for Astroparticle Physics (HAP), Research Department of Plasmas with Complex Interactions (Bochum), Germany; Fund for Scientific Research (FNRS-FWO), FWO Odysseus programme, Flanders Institute to encourage scientific and technological research in industry (IWT), Belgian Federal Science Policy Office (Belspo); University of Oxford, United Kingdom; Marsden Fund, New Zealand; Australian Research Council; Japan Society for Promotion of Science (JSPS); the Swiss National Science Foundation (SNSF), Switzerland; National Research Foundation of

Korea (NRF); Danish National Research Foundation, Denmark (DNRF).

Facilities: ANTARES, IceCube.

REFERENCES

- Aartsen M. G., Abbasi R., Abdou Y. et al. (IceCube Collaboration) 2013a, Phys. Rev. Lett., 111, 021103.
- Aartsen, M. G., et al. (IceCube Collaboration) 2013b, Phys. Rev. Lett., 113, 101101.
- Aartsen, M. G., et al. (IceCube Collaboration) 2013c, Sci, 342, 1242856.
- Aartsen M. G., Abbasi R., Abdou Y. et al. (IceCube Collaboration) 2013d, ApJ, 779, 132.
- Aartsen M. G., Ackermann M., Adams J. et al. (IceCube Collaboration), 2015, Phys. Rev. D, 91, 022001.
- Abbasi, R., Abdou, Y., Abu-Zayyad, T., et al. (IceCube Collaboration) 2010, NIMPA, 618, 139.
- Abbasi, R. et al. (IceCube Collaboration) 2011, ApJ, 732, 18.
- Abbasi, R. et al. (IceCube Collaboration) 2012, ApP, 35, 10, 615.
- Achterberg, A., Ackermann, M., Adams, J., et al. (IceCube Coll.) 2006, APh, 26, 155.
- Adrian-Martinez S., Samarai I. Al, Albert A. et al. (ANTARES Collaboration) 2012a, Phys. Lett. B, 714, 224.
- Adrian-Martinez S., Samarai I. Al, Albert A. et al. (ANTARES Collaboration) 2012b, ApJ, 760, 53.
- Adrian-Martinez S., Samarai I. Al, Albert A. et al. (ANTARES Collaboration) 2013a, JCAP, 1303, 006.
- Adrián-Martínez S., Samarai I. Al, Albert A. et al. (ANTARES Collaboration) 2013b, Eur. Phys. J. C, 73, 2606.
- Adrián-Martínez S., Albert A., André M., et al. (ANTARES Collaboration) 2014, ApJ, 786, L5.
- Ageron M., Aguilar J. A., Samarai I. Al et al. (ANTARES Collaboration) 2011, Nucl. Instrum. Meth., A 656, 11.
- Ahlers M., Bai Y., Barger V. & Lua R., 2015, arXiv:1505.03156v1.
- Ahrens J., Andrés E., Bai X. et al. 2002, Phys. Rev. D, 66, 012005
- Alvarez-Muñiz J. & Halzen F., 2002, ApJ, 576, L33.

- Anchordoqui L. A. et al., 2014a, Phys. Rev. D, 89, 083003.
- Anchordoqui L. A. et al., 2014b, Phys. Rev. D, 90, 123010.
- Atoyán A. & Dermer C.D., 2001, Phys.Rev.Lett. 87, 221102.
- Aynutdinov V., Avrorin A., Balkanov V. et al. 2008, Nucl.Instrum.Meth. A588, 99.
- Bai Y. et al., Phys. Rev. D, 2015, 90, 063012.
- Blandford, R.D. & Ostriker, J.P, 1978, ApJ, 221, L29.
- Becker J. K., 2008, Physics Reports, 458, 173.
- Becker J. K., Biermann P. L. & Rhode W., 2005, ApP, 23, 4, 355.
- Becker J. K., Stamatikos M., Halzen F. & Rhode W., 2006, ApP, 25, 2, 118.
- Bednarek W., 2005, ApJ, 631, 1.
- Cavasinni V., Grasso D. & Maccione L., 2006, ApP, 26, 41.
- Cholis I. & Hooper D., 2013, JCAP, 06, 030.
- Eichmann B., Schlickeiser R. & Rhode W., 2012, AAS, 749, 2.
- Fujita Y., Kimura S. S. & Murase K., 2015, Phys. Rev. D, 92, 023001.
- Gaisser T. K., Halzen F. & Stanev T., 1995, Phys.Rept., 258, 173
- González-García M. C., Halzen F., Niro V, 2014, ApP, 57, 39.
- Guetta D. & Amato E., 2003, ApP, 19, 403.
- Halzen F. & Hooper D., 2002, Rept. Prog. Phys. 65, 1025.
- Halzen F., Kappes A. & Murchadha A., 2008, Phys. Rev. D, 78, 063004.
- Hümmer S., Baerwald P. & Winter W., 2012, Phys. Rev. Lett., 108, 231101.
- Kappes A., Hinton J., Stegmann C. & Aharonian F. A., 2007, ApJ, 656, 870.
- Kalashov O. E., Kusenko A. & Essey W., 2013, Phys. Rev. Lett., 111, 041103.
- Kelner S.R. & Aharonian F.A., Phys. Rev. D, 2008, 78, 034013.
- Kistler M. D. & Beacom J. F., 2006, Phys. Rev. D, 74, 063007.
- Krymskii G.F., 1977, Soviet Physics Doklady, 22, 327.
- Learned J. G. & Mannheim K., 2000, Annu. Rev. Nucl. Part. S., 50, 679

- Levinson A. & Waxman E., 2001, *Phys. Rev. Lett.* 87, 171101.
- Mandelartz M. & Becker Tjus J., 2015, *ApP*, 65, 80.
- Mannheim K., 1995, *ApP*, 3, 295.
- Mészáros P. & Waxman E., 2001, *Phys. Rev. Lett.*, 87, 171102.
- Mücke A., Protheroe R. J., Engel R., Rachen J. P. & Stanev T., 2003, *ApP*, 18, 6, 593.
- Murase K. et al, 2006, *ApJ*, 651, L5.
- Murase K. & Nagataki S., 2006, *Phys. Rev. Lett.*, 97, 051101.
- Murase, 2015, *AIP Conf.Proc.* 1666, 040006.
- Nellen L., Mannheim K. & Biermann P. L., 1993, *Phys. Rev. D.*, 47, 5720.
- Neyman J, 1937, *Phil. Trans. Royal Soc. London A*, 236, 333.
- Fox D. B., Kashiyama K. & Mészáros P., 2013, *ApJ*, 774, 74.
- Padovani P. & Resconi E., 2014, *MNRAS*, 443, 474.
- Rachen J. P. & Mészáros P., 1998, *Phys. Rev. D.*, 58, 123005.
- Roulet E., Sigi G., van Vliet A. & Mollerach S., 2013, *JCAP*, 01, 028.
- Romero G.E., Torres D.F., Kaufman Bernadó M. M. & Mirabel I. F., 2003, *A&A*, 410, L1.
- Razzaque S., Mészáros P. & Waxman E., *Phys. Rev. D*, 68, 083001.
- Razzaque S., 2013, *Phys. Rev. D*, 88, 081302.
- Stecker F. W., Done C., Salamon M. H. & Sommers P., 1991, *Phys. Rev. Lett.*, 66, 2697.
- Stecker F. W., 2005, *Phys. Rev. D*, 72, 107301.
- Stecker F. W., 2013, *Phys. Rev. D*, 88, 047301.
- Torres D.F., Romero G.E & Mirabel F., 2005, *Chin. J. Astron. Astrophys.*, 5, 183.
- Vissani F., Aharonian F. & Sahakyan N., 2011, *Astropart.Phys*, 34, 778.
- Waxman E. & Bahcall J., 1997, *Phys. Rev. Lett.*, 78, 2292.
- Waxman E. & Bahcall J., 1999, *Phys.Rev.D*, 59, 023002.
- Waxman E. & Bahcall J., 2000, *ApJ*, 541, 707.